Nano Energy 72 (2020) 104676

Contents lists available at ScienceDirect

Nano Energy

journal homepage: http://www.elsevier.com/locate/nanoen

All 3D-printed stretchable piezoelectric nanogenerator with non-protruding kirigami structure

Xinran Zhou [a,b], Kaushik Parida [a], Oded Halevi [a,b,c], Yizhi Liu [d], Jiaqing Xiong [a], Shlomo Magdassi [b,c,**], Pooi See Lee [a,b,*]

[a] School of Materials Science and Engineering Nanyang Technological University, 50 Nanyang Avenue, Singapore, 639798, Singapore
[b] Singapore-HUJ Alliance for Research and Enterprise (SHARE), Nanomaterials for Energy and Water Nexus (NEW), Campus for Research Excellence and Technological Enterprise (CREATE), 1 Create Way, Singapore, 138602, Singapore
[c] Casali Center of Applied Chemistry Institute of Chemistry, The Hebrew University of Jerusalem, Jerusalem, 91904, Israel
[d] Department of Astronautic Science and Mechanics, Harbin Institute of Technology, No.92, Xidazhi Street, Harbin 150006, China

ARTICLE INFO

Keywords:
Piezoelectric nanogenerator
Stretchable
Kirigami
3D printing
Gait analysis
Direct-write printing

ABSTRACT

With the advancement of wearable electronics, stretchable energy harvesters are attractive to reduce the need of frequent charging of wearable devices. In this work, a stretchable kirigami piezoelectric nanogenerator (PENG) based on barium titanate ($BaTiO_3$) nanoparticles, Poly(vinylidene fluoride-co-trifluoroethylene) (P(VDF-TrFE)) matrix, and silver flakes-based electrode is fabricated in an all-3D printable process suited for additive manufacturing. The 3D printable extrusion ink is formulated for facile solvent evaporation during layer formation to enable heterogenous multilayer stacking. A well-designed modified T-joint-cut kirigami structure is realized to attain a non-protruding, high structural stretchability performance, overcoming the out-of-plane displacement of the typical kirigami structure and therefore enabling the pressing-mode of a kirigami-structured PENG. This PENG can be stretched to more than 300% strain, which shows a great potential for application in wearable electronic systems. Furthermore, a self-powered gait sensor is demonstrated using this PENG.

1. Introduction

The rapidly advancing electronic industry is changing our way of working and living, in which energy supply is the most fundamental need [1,2]. Due to resources limitations and environment pollution issues caused by traditional energy generation, and the inconvenience in repeatedly charging of electronic devices [3–5], the mobile electronic systems require an effective, sustainable, autonomous and portable energy supply [6,7]. Among all forms of energy sources, mechanical energy is one of the most available form of energy in our daily life. From the vibration of machines, to the mechanical energy of wind, water flow or rain drop, or the motion of human body, mechanical energy can be found everywhere. Converting mechanical energy to electricity to power portable electronic systems is a simple, sustainable, and reliable choice. Amongst the mechanical energy harvesting principles, piezoelectric effect and triboelectric effect are suitable for portable energy harvesters [8–17]. Triboelectric nanogenerator (TENG) is based on triboelectric effect and electrostatic induction. While triboelectric effect is a phenomenon that a material becomes electrically charged after it contacts a different material, piezoelectric effect is based on the inherent polarizations of materials [15,18,19]. Thus, piezoelectric energy harvesters are stable, reliable and not affected by environmental factors such as humidity [20–24]. Piezoelectric nanogenerator (PENG) is defined as piezoelectric energy harvester that uses nanomaterials or thin film structure for the energy conversion [11,25–28]. Piezoelectric materials include single crystals such as quartz [29], polycrystalline ceramics (lead zirconate titanate, barium titanate, etc.) [29], or metalloids such as tellurium [30], 2D materials such as MoS_2 (with piezoelectric constant d_{11} along the armchair direction that is 1.5 times greater than that of quartz [31,32]), and a few types of polymers that are flexible [33]. One of the most important piezoelectric polymer is P(VDF-TrFE) that has been proven to have a higher piezoelectricity than PVDF due to the

* Corresponding author. School of Materials Science and Engineering Nanyang Technological University, 50 Nanyang Avenue, Singapore, 639798, Singapore.
** Corresponding author. Singapore-HUJ Alliance for Research and Enterprise (SHARE), Nanomaterials for Energy and Water Nexus (NEW), Campus for Research Excellence and Technological Enterprise (CREATE), 1 Create Way, Singapore, 138602, Singapore.
E-mail addresses: magdassi@mail.huji.ac.il (S. Magdassi), pslee@ntu.edu.sg (P.S. Lee).

https://doi.org/10.1016/j.nanoen.2020.104676
Received 26 September 2019; Received in revised form 5 March 2020; Accepted 6 March 2020
Available online 9 March 2020

thermodynamically favored crystallization of the ferroelectric β phase induced from the extra fluorine atom in each repeating unit [34]. In addition, the incorporation of nanoparticles into piezoelectric polymer P(VDF-TrFE) leads to constrains in polymer chains, therefore enhancing the crystallization and polarization of the polymer [35,36].

The emerging trend for electronics is wearable technology that enable hands-free information collection and exchange. Human skin has around 30% strain during body movement [37], in order to achieve a comfortable human-machine interface, and to integrate with other wearable energy storage and energy consuming devices, mechanical energy harvesters are required to be stretchable to function in wearable devices. The stretchability of piezoelectric energy harvester is achieved in several ways, this includes buckling, weaving, cutting, micro-pattern designing, and compositing with elastomer. Early in 2011, Qi et al. used pre-strain polydimethylsiloxane (PDMS) to transform lead zirconate titanate (PZT) ribbons into wave-like buckled form [38]. The buckling provided 8% strain in the material. In addition to PZT ribbons, polyvinylidene difluoride (PVDF) fibers could also be buckled on pre-strain PDMS to achieve 30% strain [39]. Subsequently, PVDF nanofibers were deposited onto pre-strained PDMS coated Ecoflex substrate by helix electrohydrodynamic printing (HE-Printing) with a fractal inspired architecture, causing 200% stretchability [40]. Weaving is another method to make piezoelectric energy harvester stretchable. Yun et al. achieved 20% strain by weaving PVDF film with polyester and silicone tube [41]. For micropatterning method, Lee et al. designed the micro-line pattern structured carbon nanotube (CNT)/PDMS and spin-coated poly(vinylidene fluoride-co-trifluoroethylene) (P(VDF-TrFE)) on it [42]. The resultant microstructure made it flexible and stretchable to 30% strain. Piezoelectric composite with elastic matrix is also an effective choice for high stretchability. Jeong et al. fabricated a composite of PMN-PT particles, CNT, and silicone matrix and made it into a hyper-stretchable energy harvester [43]. It stretched to 200% maximum strain. We have reported a stretchable and transparent hybrid (piezoelectric and triboelectric) nanogenerator with PDMS and barium titanate nanoparticles ($BaTiO_3$ NPs) that has an elasticity of 60% strain [23]. Recently, Zhou et al. and Niu et al. reported stretchable PENGs based on PZT filler and silicone rubber matrix for energy harvesting and self-powered motion monitoring with high output [44,45]. In Zhou et al. 's work, the device could sustain 50 – 200% strain [44]. In Niu et al.'s study, the maximum strain for the PZT/rubber composite is 575%, and the device could work stably under 30% strain [45].

A concern on the above methods in tailoring stretchability is the decrease of the effective content of piezoelectric material and therefore the overall reduction in piezoelectric output. In addition, complex steps involving multiple processing techniques are required to fabricate a device with the methods mentioned above, which limits the facile fabrication and scalability. To avoid the decrease of piezoelectric material content and complex materials processing, an effective technique for fabricating stretchable piezoelectric energy harvester is by kirigami cutting. This method has an advantage in mass production of stretchable piezoelectric harvesters because it can retain the optimum material compositions and it avoids complex fabrication processes. It is a simple but effective way to create stretchable device by using intrinsically flexible materials. Hu et al. cut kirigami patterns on PVDF thin films, resulting in 30% maximum strain [46]. This simple stretching kirigami structure is able to sustain large strain so it is widely adopted in other devices such as supercapacitors, solar cells, and strain sensors [47–50]. However, the simple stretchable kirigami structure typically functions by tilting out of the plane and bending, so that part of the structure protrudes out under stretching, which makes the structure unsuitable to operate under compression or pressing mode. Since the 3-3 mode (force is subjected in the direction vertical to the piezoelectric film, and electric signals collected in the direction vertical to the piezoelectric film) of piezoelectric effect usually has the highest piezoelectric constant, pressing mode is the most common and effective mode for piezoelectric energy harvesters. Even though the kirigami structure enables the stretchability, its use in energy harvester is limited due to the constraint of physical protrusions from the kirigami structure. In this work, a modified kirigami structure is designed to realize piezoelectric energy harvesters that are highly stretchable with minimal structural protrusions, therefore avoiding the impairment in performance during pressing or compression mode.

As a type of rapid prototyping technique, 3D printing is effective in fabricating complex three-dimensional (3D) structures with computer modelling, which enables it to revolutionize the traditional manufacturing industry. By introducing 3D printing technique into the manufacturing of this kirigami stretchable piezoelectric energy harvester, it allows rapid prototyping for fabrication of complex three-dimensional (3D) structures of any designed shape in single step, low cost and efficient manner, in which cutting and mould fabrication can be eliminated [44–57]. This capability enables the possibility of integrating 3D printable 3D structured materials into the whole electronic system. Until now, no 3D printed stretchable piezoelectric energy harvesters have been reported due to the lack of stretchable piezoelectric materials and electrode materials that are compatible with the 3D printing process (an analysis of the state-of-art 3D printed piezoelectric materials and devices is shown in Table S1). Through the design of a modified kirigami structure to achieve stretchability, we are able to use a formulated printable composite material system for a facile 3D printing method to fabricate stretchable PENG. In direct write 3D printing method, the layer formation can be achieved using thermal fusing, UV-curing, solvent evaporation. The printable PVDF-TrFE here adopts the facile solvent evaporation method. It is noted that the solvent evaporation printing often suffers from dissolution of the prior layers and shrinkage during evaporation upon 3D printing. Herein, our formulated 3D printed ink is prepared using a fast evaporating solvent with low thermal budget requirement to achieve a homogenous printed layer with defined interface.

In this work, we realize the well-designed modified kirigami structure by direct-write 3D printing process. By developing the piezoelectric ink and the conductive ink, an all-3D printed piezoelectric energy harvester is demonstrated for the first time. $BaTiO_3$ nanoparticles reinforced P(VDF-TrFE) is used as the piezoelectric material for enhanced piezoelectricity comparing with neat P(VDF-TrFE). Silver (Ag)-based conductive layers are 3D printed on the piezoelectric film as electrodes. The all-3D printed kirigami PENG device is demonstrated as a wearable energy harvester to harvest energy from body motion.

2. Results and discussion

Fig. 1 schematically describes the printing and poling process of the piezoelectric device. First, the piezoelectric $BaTiO_3$ NP/P(VDF-TrFE) ink was printed on a piece of ITO glass that serves as the bottom electrode during the poling process. Five layers were printed to form a 40 μm thick sample. The thickness of one layer was measured with a surface profiler to be 8 μm. Conductive Ag flake/P(VDF-TrFE) ink was then printed on the top of the printed piezoelectric structure as the top electrode. The same matrix material enables the good compatibility between the piezoelectric material and the electrode. The printed structure and the ITO glass substrate was put into silicone oil and poled with high electric field under 100 °C for 2 h, for the alignment of the ferroelectric dipoles inside the P(VDF-TrFE) matrix and the $BaTiO_3$ NPs. Then, the silicone oil was removed and the sample was peeled from the substrate, flipped over, and fixed on the substrate again for the bottom electrode printing. Finally, a bottom electrode was printed using the same Ag flake/P(VDF-TrFE) conductive ink to achieve the all 3D printable PENG.

In P(VDF-TrFE), the piezoelectricity comes from β phase. The existence of β phase in the 3D printed and thermal-treated P(VDF-TrFE) samples is confirmed with XRD (Fig. 2a inset). The peak at $2\theta = 19.6°$ represents the β phase of P(VDF-TrFE), and the peaks representing α phase are not present, confirming the P(VDF-TrFE) fabricated by

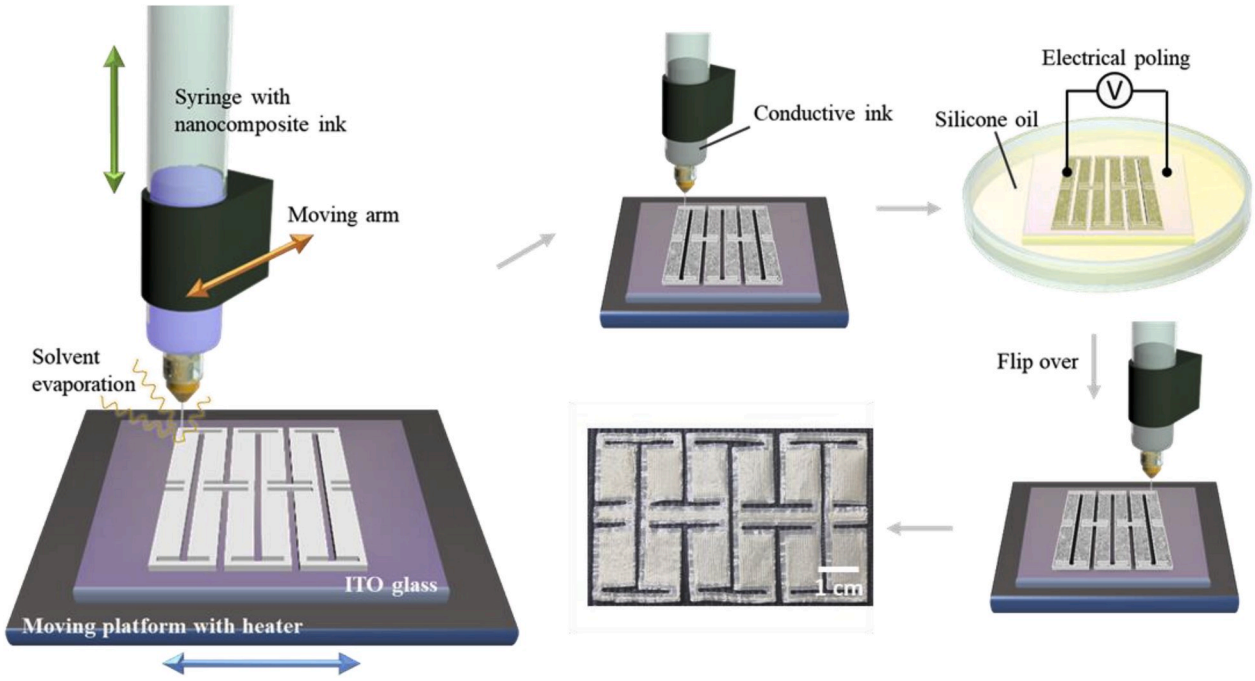

Fig. 1. Schematic of the fabrication process of the all 3D-printed PENG.

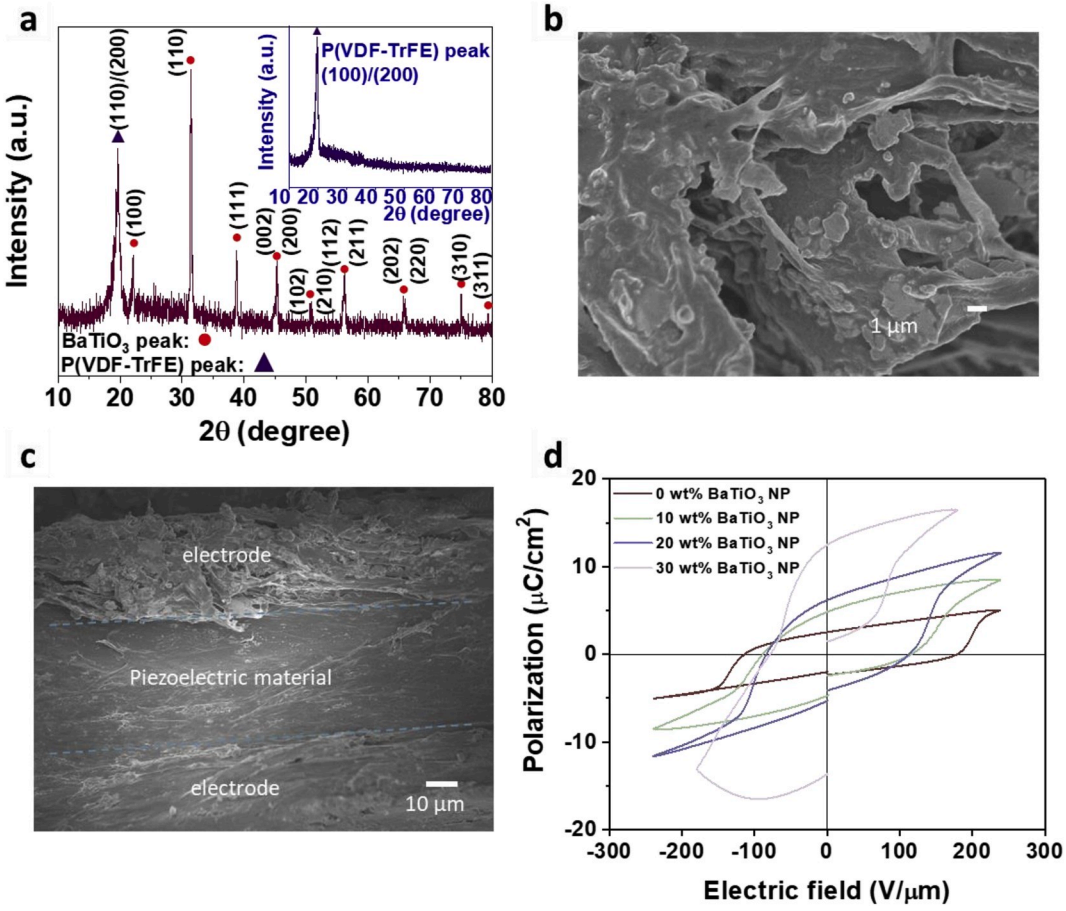

Fig. 2. The inset of (a) is the XRD spectra of the 3D printed pure P(VDF-TrFE) and after annealing at 120 °C for 2 h, and (a) 3D printed $BaTiO_3$ NP/P(VDF-TrFE) composite with 20 wt% $BaTiO_3$ NPs and after annealing at 120 °C for 2 h. SEM image of (b) 3D-printed Ag flake/P(VDF-TrFE) electrode and (c) SEM image of interface of Ag flake/P(VDF-TrFE) top electrode, piezoelectric material $BaTiO_3$ NP/P(VDF-TrFE), and Ag flake/P(VDF-TrFE) bottom electrode. (d) P-E loop of spin coated $BaTiO_3$ NP/P(VDF-TrFE) samples with $BaTiO_3$ content of 0%, 10 wt%, 20 wt%, and 30 wt%.

printing and annealing contains primarily the ferroelectric β phase. After mixing of $BaTiO_3$ NPs and P(VDF-TrFE), both materials maintain the ferroelectric phases as shown in the XRD spectrum of the 3D printed and thermal-treated composite sample with 20 wt% of $BaTiO_3$ NPs (Fig. 2a, Fig. S1, elaborated in S1). From the FTIR spectrum (Fig. S2, elaborated in S2), it can be concluded that with the addition of $BaTiO_3$ NPs, the phase composition of P(VDF-TrFE) is not affected and the piezoelectric β phase dominants.

To form a PENG device, top and bottom electrodes need to be attached onto the piezoelectric film. In this work, Ag flake/P(VDF-TrFE) was used as the electrode material, whose resistivity is around 44.3 MΩ m with a standard deviation of 1.32 MΩ m, as measured by 4-probe method and calculated according to the sample thickness. The Ag flakes and the P(VDF-TrFE) were dissolved in MEK and 3D printed onto the printed $BaTiO_3$/P(VDF-TrFE) film. SEM imaging was conducted to check the morphology of the electrode and the interface between electrodes and the piezoelectric material (Fig. 2b–c, Fig. S3). The morphology of the electrodes is shown in Fig. 2b. Silver flakes of different sizes were distributed inside the P(VDF-TrFE) matrix forming a conductive percolative connection. From Fig. 2c, the electrode layers have a clear interface with the piezoelectric layer and the silver flakes are well contained in the top electrode due to controlled fast evaporation of the solvent during printing of the electrode. This also indicates that the 3D printing of the electrode is highly feasible for the preparation of multilayer sample with potential to reduce the number of processing steps and equipment required in manufacturing.

Apart from confirming the piezoelectric phases, piezoelectric characterizations including piezoelectric coefficient (d_{33}) measurements and polarization-electric field loop (P-E loop) measurements were done on the 3D printed samples. A film sample with 20 wt% $BaTiO_3$ NP content was 3D printed and poled with 50 V/μm electric field according to its average thickness (of 40 μm). The d_{33} of the sample was measured as – 20 pC/N (standard deviation is 0.60 pC/N for three 20 wt% $BaTiO_3$ samples). In comparison, the d_{33} of the 3D printed pure P(VDF-TrFE) sample that went through the same fabrication process and the same poling electric field is – 16 pC/N (standard deviation is 0.55 pC/N for three samples). The P-E loop measurements were done on the samples with $BaTiO_3$ NP concentrations from 0% to 30 wt%, as shown in Fig. 2d. The P-E loop of the same $BaTiO_3$ NP with non-piezoelectric matrix (20 wt% in polyurethane acrylate) was tested as a reference, shown in Fig. S4. From the P-E loop, the coercive field, saturation polarization, and residual polarization of the samples in each concentration can be obtained. In Fig. 2d, from 0% to 20 wt% $BaTiO_3$ NP concentration, the P-E loop is symmetric, and it is a typical shape for ferroelectric material under saturation field condition. However, the P-E loop of 30 wt% $BaTiO_3$ NP is consistently asymmetric, indicating the presence of large amount of defects in the layer. Additionally, 0%, 10 wt%, and 20 wt% samples are tested under an electric field of 240 V/μm. The 30 wt% sample suffers from electrical breakdown when the electric field is larger than 180 V/μm, which is also an indication of a large amount of defects caused by higher amount of fillers or more interfacial defects between the P(VDF-TrFE) matrix and the $BaTiO_3$ NP reinforcement. Thus, 30 wt % $BaTiO_3$ NP is not considered in the following studies. It can also be observed that the residual polarization and the saturation polarization both increase with increasing $BaTiO_3$ content, and the coercive field decreases with increasing $BaTiO_3$ NP content, which all show that the piezoelectricity improves with increasing $BaTiO_3$ NP content. The P-E loop result proves that the piezoelectricity of P(VDF-TrFE) improved by the addition of piezoelectric $BaTiO_3$ NPs. This improvement can be due to several reasons. First, $BaTiO_3$ NPs have a larger piezoelectric coefficient than P(VDF-TrFE). By compositing the two materials, the piezoelectric properties are contributed from both phases and proved to be better than the neat P(VDF-TrFE). As ceramic particles, the high dielectric constant (~4000) [58] of $BaTiO_3$ nanoparticles could concentrate the electric field onto the surrounding P(VDF-TrFE) matrix with low dielectric constant (~11) [59]. Another reason for the enhancement of piezoelectricity is the concentration of stress. By adding $BaTiO_3$ NPs, the stiffness of the sample is enhanced and the fracture strain decreases (Fig. S5), indicating the ability of the matrix to sustain larger local stresses.

To characterize the energy harvesting performance of the PENG, measurement was done with a printed square film sample (2 cm × 2 cm, an effective area of 1 cm × 1 cm). The measurement setup and circuit are shown in Fig. S6. The sample was fixed on the supporting stand with a force sensor and pressed under 60 N force by a magnetic shaker with a frequency of 5 Hz. The voltage output and current output under different external resistance were tested, and the power output was calculated. As shown in Fig. 3a, this device can generate a voltage of more than 6 V under 60 N force exerted at a frequency of 5 Hz. The current density under the same testing condition is 2 $\mu A/cm^2$, shown in Fig. 3b. The voltage and current density showed the good energy harvesting ability of this device and confirmed the effectiveness of this material system and poling process. The voltage and current output under different load resistance are measured (Fig. 3c). The output voltage increases with the load resistance and the output current density decreases with the load resistance, which agrees with Ohm's law. The power density is also calculated by multiplying the voltage and the current density, and the relationship between power density and the load resistance is plotted in Fig. 3d. The largest power density 1.4 $\mu W/cm^2$ is obtained when the load resistance is 10^7 Ω for 20 wt% $BaTiO_3$ sample, which agrees with the impedance matching principle according to the impedance measurement results as shown in Fig. S7. Moreover, the output voltage at different force (20 N, 40 N, and 60 N) and different frequencies (5 Hz, 10 Hz, 15 Hz) were measured for 0 wt%, 10 wt%, and 20 wt% $BaTiO_3$ samples (Fig. 3e and f). The output voltage increases with increasing force and frequency for all the samples. To demonstrate the charging ability of the device, experiments were done to use the PENG to charge a 1 μF capacitor (Fig. 3g). By hand tapping, the capacitor can be fully charged in 15 s. The device is also able to drive light emitting diodes (LED). Supporting video 3 and Fig. 3h shows that 3 LEDs that were connected in series can be powered by the PENG by hand tapping. The cycling stability was tested by applying 60 N force at 5 Hz frequency to a 20 wt% $BaTiO_3$ PENG device for 3000 times (Fig. S8). Only minor variation occurred during the testing period, which indicates the performance of the PENG is stable. The testing signals are proven to be from piezoelectric effect rather than other sources as validated by the following two experiments. In the first experiment, a non-poled 20 wt% $BaTiO_3$/P(VDF-TrFE) sample was measured under the same testing conditions (60 N, 5 Hz). The voltage and current output shown in Fig. S9 were negligible compared to the poled sample, indicating the measurement setup is efficient in preventing other source of signals and verified that the results shown in this paper is from piezoelectric effect. The second experiment is to reversely connect the measurement component to the two electrodes of the sample (20 wt% $BaTiO_3$/P(VDF-TrFE), under 50 N, 5 Hz force). Due to the nature of piezoelectric effect, the signal should also be inversed. The result was shown in Fig. S10, proving that the signal totally comes from piezoelectric effect.

Supplementary video related to this article can be found at https://doi.org/10.1016/j.nanoen.2020.104676

After confirming the piezoelectricity and the energy harvesting properties of the 3D printed PENG, the device structures are designed to achieve high stretchability using kirigami strategy (Fig. 4a–f). The standard typical stretching kirigami structure (Fig. 4a) is widely used to make intrinsically flexible film highly stretchable by tilting the direction of each repeating structure segment to partially perpendicular to the stretching direction and make them bend in the stretching direction. That means the structure must protrude out of plane during stretching, making it not possible to operate or compress it from the normal direction (Fig. 4d). Majority of the mechanical energy harvester uses the 3-3 mode of energy generation, at which the pressure is applied in the normal direction to the energy harvester, and the electric output from the same direction is harvested. This is the most efficient way of energy

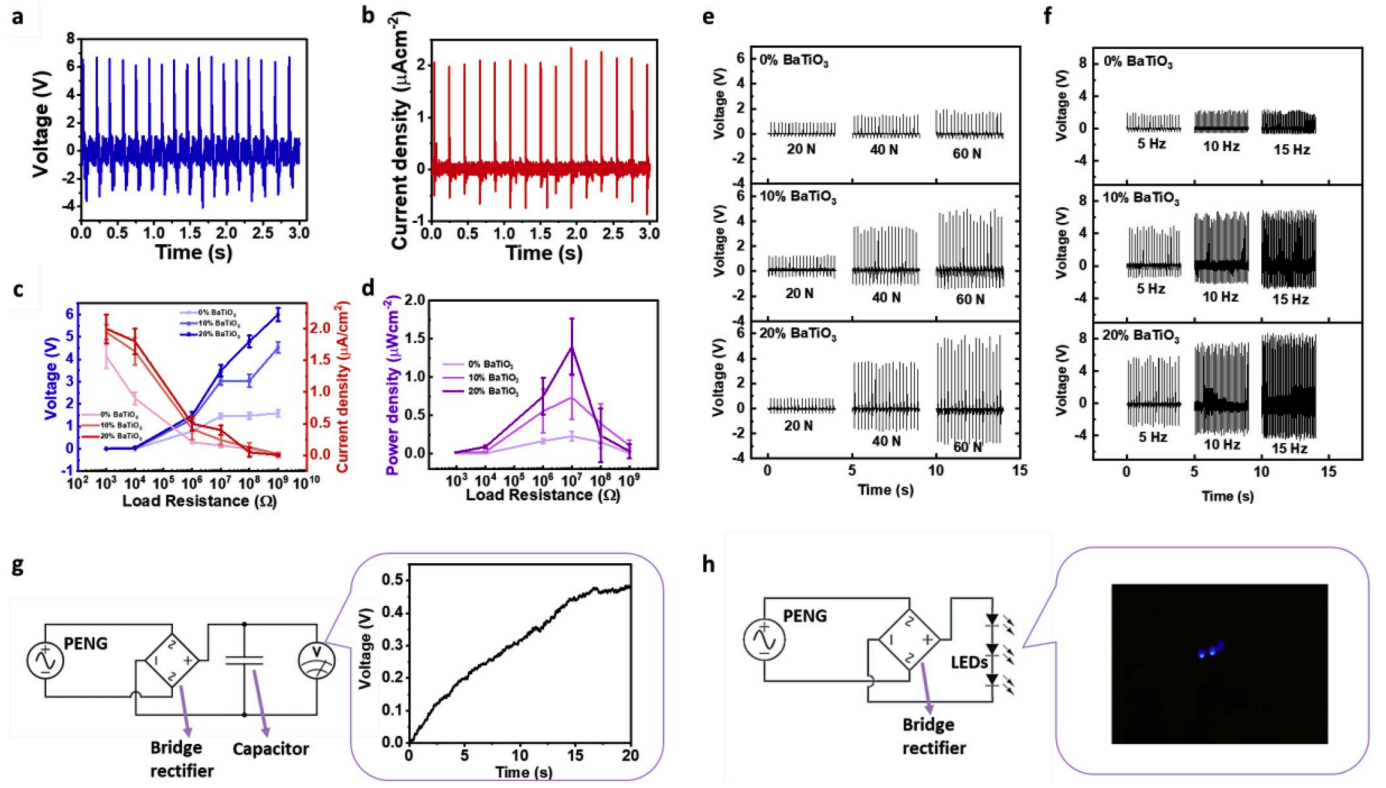

Fig. 3. (a) Output voltage and (b) current density of printed 20 wt% $BaTiO_3$ NP/P(VDF-TrFE) based piezoelectric energy harvester under 60 N force and 5 Hz frequency with an effective area of 1 cm^2. (c) Voltage and current density versus load resistance for 0 wt% to 20 wt% $BaTiO_3$ NP/P(VDF-TrFE) samples. (d) Power density versus load resistance. (e) Voltage output at different force (under 5 Hz frequency). (f) Voltage output at different frequency (under 60 N force). (g) PENG charging a capacitor. (h) PENG powering 3 LEDs that are connected in series.

generation because the d_{33} is usually higher than d_{31} and d_{12}. Energy harvesting by pressing is also safer for the device compared to stretching because it is more resistant to damage when subjected to pressing.

To overcome the limitation of the kirigami structure and to enable the energy harvester in generating energy in 3-3 direction, modifications were made based on the kirigami structure to impede protrusions out of plane under stretching. Perpendicular cuttings were introduced on each end of the long cutting without joining point, as shown in Fig. 4b. This cutting manner, as the unit cell of a fractal cut structure, was well studied and used for increasing the compliance of material [60]. In the following discussion, we refer this structure to fractal-cut kirigami. Each corner of the rectangles in fractal-cut kirigami plays a role as the rotation centre so that the rectangles can rotate around the corners and the whole structure can expand. Fig. 4c shows the structure specifically designed in this work, termed as T-joint-cut. It has short cuttings that are in perpendicular directions with the long cuttings and connected with the long cuttings with joining points at the long ends. In this way, the overall tilting and bending can be transformed into the minor bending at each small joint, and other parts of the structure can rotate about the joint to achieve high stretchability even when the whole structure except for the small joints are confined into the original plane (Fig. 4e and f). Even the joints may protrude slightly out under large stretching, the displacement is minor and not affecting the functioning of the device. Fig. 4g and h shows the top view and side view of the out-of-plane protrusion at the joint area for the T-joint-cut kirigami under 45° opening of the cutting by tilting around the joint. In this condition, the protrusion is only 2.6 mm, and when the cutting opens to 90°, the protrusion is 3.7 mm as shown in Fig. 4i and j. In comparison, if the original kirigami structure is confined into the original plane with only a minor displacement allowed, it will lose most of its stretchability.

Finite element modelling (FEM) analysis was done with the three structures to understand their behaviour under stretch when confined in a plane, which is a similar condition to the working condition of a wearable PENG. The three structures were designed with the same size (10 cm × 10 cm), width of repeating unit (22 mm), distance between the end of one cutting and the edge or another cutting (2 mm) and the width of the cutting line (1 mm). In the FEM analysis, all the structures are constrained with all degrees of freedom on the left surface and constrained with zero displacement in z-direction. The constraint in z-direction is to limit the variable toonly the x displacement, which makes it clear for comparing the behaviour of the three structures. 200 Pa pressure was applied on the right surface of all the structures along + x direction. With the same constraint and pressure applied to the three models, the displacement is simulated by FE modelling and shown in Fig. 4k-m. Comparing the displacement distribution and displacement of the three structures, the typical kirigami structure has little displacement under the pressure because this structure is not designed for in-plane deformation. The fractal-cut kirigami is slightly better than the typical kirigami because a set of joints are designed for in-plane rotation but the force in y direction is absent for opening the small cuttings. In this structure, only when the void is opened by the y-direction forces can it achieve the rotation around the joints. The T-joint-cut structure has the largest displacement that is 6.3 and 5.5 times of the displacement of typical and the fractal-cut kirigami, respectively under the same force. That is because the stretching can be effectively transferred to the joints to cause the bending of the joints and the rotation of the rectangles.

In terms of the overall stretchability, the maximum strain highly depends on the design of the structure such as the density of the cuts. To compare the maximum stretchability among the three structures with the same size and design parameters, calculations are done to show the strain under maximum extension (S3, Fig. S7). Comparing the theoretical maximum strain of the three structures, T-joint-cut structure designed by this work has the largest value that is 1.63 times of fractal-cut structure and 1.45 times of simple kirigami structure.

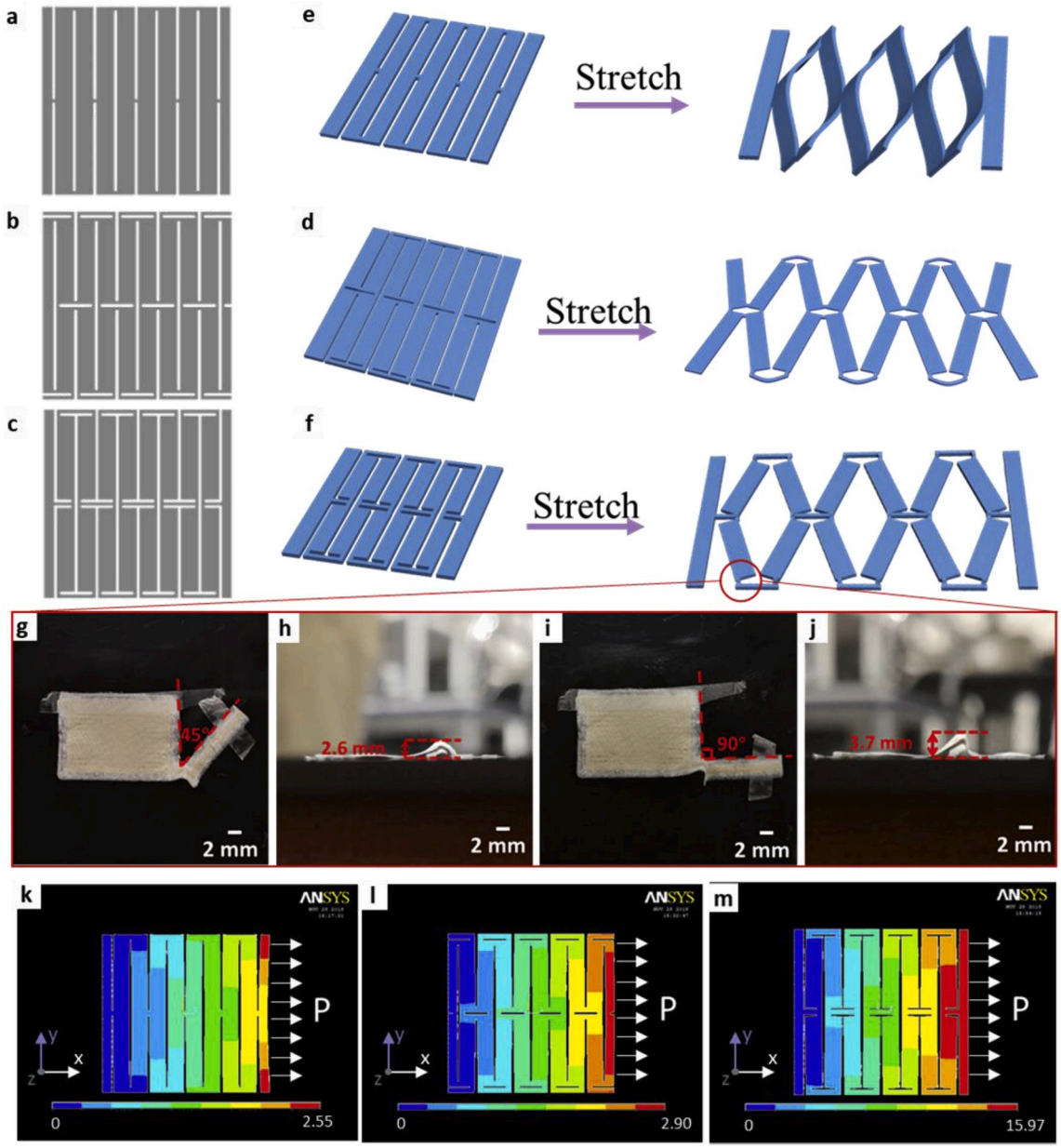

Fig. 4. Three kirigami structures: (a) simple kirigami structure, (b) fractal-cut kirigami structure and (c) T-joint-cut kirigami structure. Schematic of different stretching mode of (d) simple kirigami, (e) fractal-cut kirigami, and (f) T-joint-cut kirigami. Joint in T-joint-cut kirigami structure tilting 45° in (g) top view and (h) front view. Joint in T-joint-cut structure tilting 90° in (i) top view and (j) front view. Displacement vector sum of (k) simple kirigami, (l) fractal-cut kirigami, (m) T-joint-cut kirigami structure by FEM simulation.

From the FEM result and the maximum strain calculation, it can be concluded that the modified stretching kirigami structure that is designed in this work offers an innovative way to achieve the high stretchability by designing the 2D structure of flexible materials without protruding out of the plane. That can broaden the energy harvesting modes of stretchable energy harvesters and enable easy fabrication methods of high efficiency energy harvesters.

Since the stretchability is achieved by the rotation of rectangles about the joints, the energy output that mainly comes from the rectangle should not change after stretching. To prove this hypothesis, the voltage output of one segment of T-joint-cut kirigami structure (Fig. 5a) was mounted on the same shaker setup (Fig. 5b) and tested with different strain under 60 N force and 5 Hz frequency. As shown in Fig. 5c, for overall strain from 0% to 300%, no significant variation in voltage output is observed and the open circuit voltage output are all around 6 V which is consistent to the unstrained sample.

Taking the advantage of the steretchability and the compressibility, we also demonstrated the energy harvesting of the all-printed T-joint-cut structure PENG mounted on a wearable sock to allow conversion of the foot stamping energy into electricity. At the same time, the electric signal output can be used for sensing the gait information. Gait analysis is important for the detection of diseases and healthcare monitoring [61]. For example, nerve injury can cause the weakness of the foot and ankle dorsiflexors, leading to slap gait or steppage gait that the front part of the foot contacts the ground first followed by the heel [62]. For the recognition and rehabilitation of the gait abnormality, robot-assisted therapy is effective [63,64]. The wearable soft robotic device is an emerging field, because of their improved safety and more comfortable human-machine interface [65]. All the robotic gait rehabilitation device requires sensing elements and the sensors that usually requires constant power supply [66]. With the development of the Internet of Things (IoT) and the wireless monitoring concepts, the energy supply and recharge

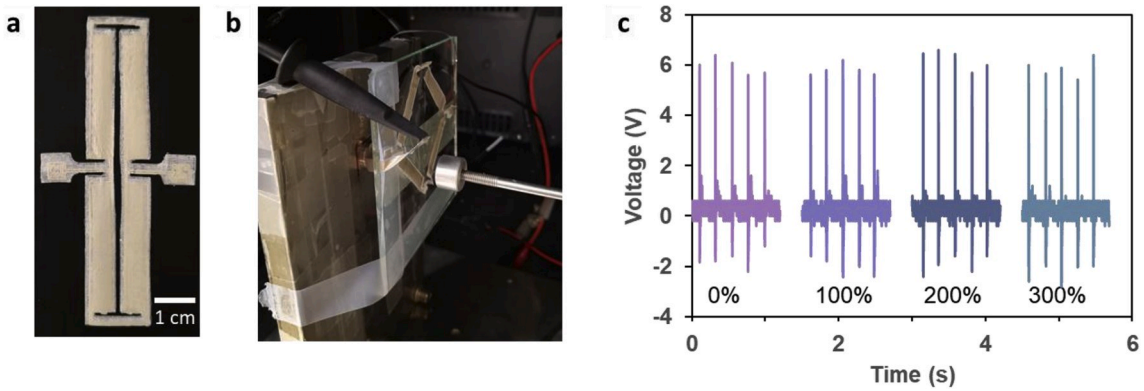

Fig. 5. (a) Printed piezoelectric energy harvester with the structure of one repeating unit of T-joint-cut kirigami structure. (b) Printed piezoelectric energy harvester mounted onto the shaker for measurement of voltage output. (c) Voltage output of printed T-joint-cut structure sample with overall strain of 0%, 100%, 200% and 300%.

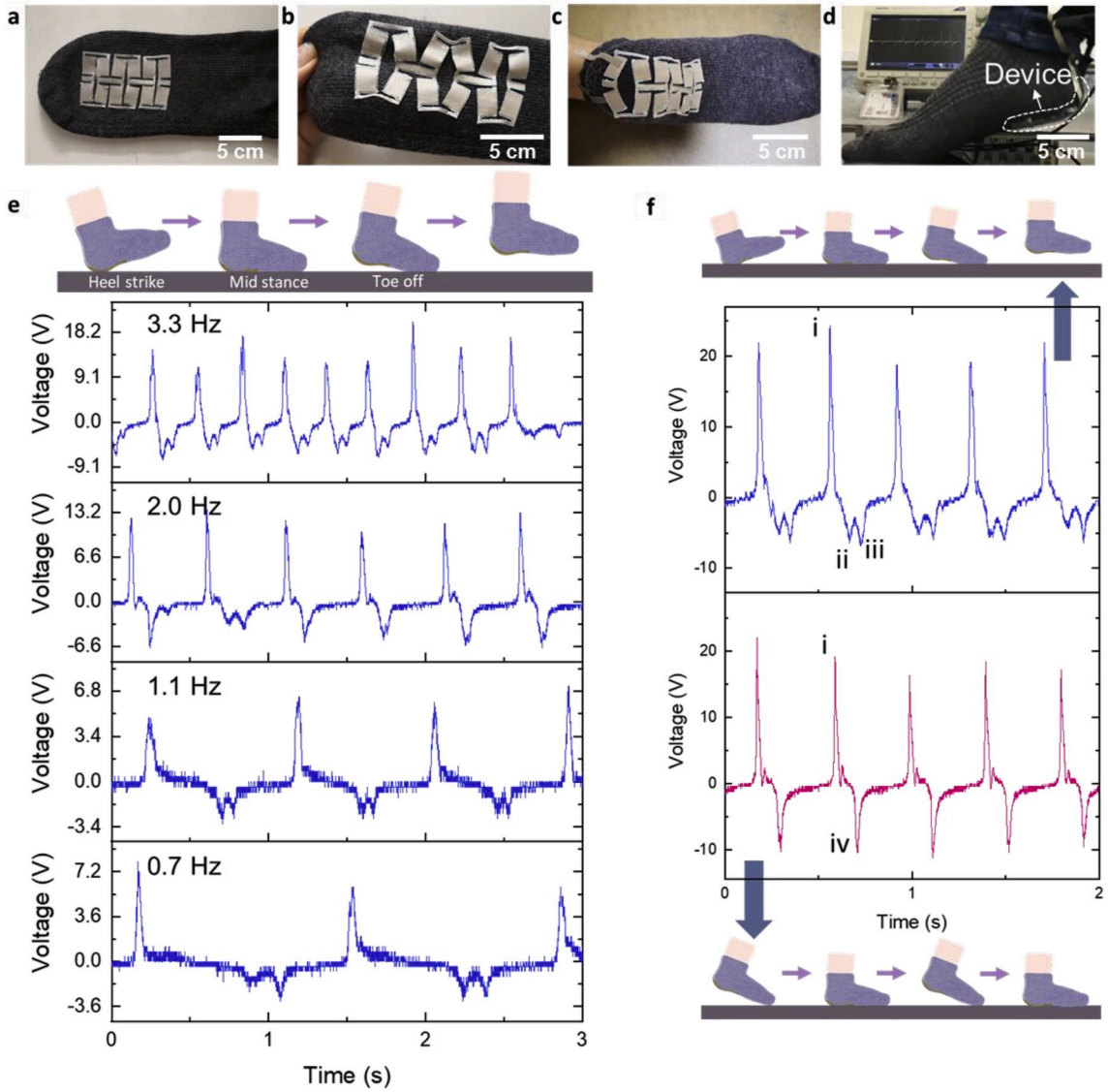

Fig. 6. (a) Optical image of the all-printed PENG mounted on a sock without stretching and (b) with stretching. (c) Photo of the all-printed PENG mounted on the heel of a sock wearing on a foot. (d) Photo of the foot stamping experiment on the printed PENG-mounted sock. (e) Schematic and voltage output of the printed PENG-mounted sock under foot stamping with different frequency and (f) different stamping posture.

requirements becomes a challenge. Different from other sensing systems, the self-powered PENG with gait sensing ability can solve the energy supply problem. Yu et al. have reported a self-powered skin--conformal piezoelectric-enhanced triboelectric nanogenerator that is able to detect the gait and other human motions without power source [67]. Adding the advantage of stretchable, our self-powered PENG is desirable for textile based gait analysis application.

The device was mounted on a sock with a small amount of adhesive (Fig. 6a). The designed kirigami structure with vertical short cuts enables the in-plane stretching of the device on the stretchable sock textile as ahown in Fig. 6b. Fig. 6c shows the wearable device mounted on the sock being worn on a foot and Fig. 6d shows the voltage output measurement from the device-mounted sock during foot stamping on the heel. When foot stamping with the device-mounted sock occurs at different frequencies, voltage signals with different frequencies and the same peak characteristics can be collected (Fig. 6e, Fig. S12). In addition, different gait manners resulted in different peak characteristics. The nature of the signal was verified in S4. As shown in Fig. 6f and Supporting videos, in normal stamping, there is one positive peak and two negative peaks (peak i – iii in Fig. 6f top). Peak i comes from the pressure when the heel strikes on the ground. After the heel strike, the weight center gradually transfers from the heel to the whole foot, which causes the opposite direction voltage output. At the same time, the front part of foot drops on the ground, causing a minor shaking of the heel part that results in a small change in the pressure on the floor. The opposite direction voltage output and the small change in pressure together forms peak ii. Then, the weight center is transferred to the front foot and the pressure at the heel reduces and this forms peak iii. When keeping (or fixing) the toes on the ground and stamping with the heel only (Fig. 6f bottom), there is one positive peak (peak i) and only one negative peak (peak iv). The peak i is the same as that in the normal stamping figure, and since there is no front foot dropping process, the reduce of pressure on the heel is continuous without disturbance. Thus, only peak iv presents in the negative direction. The results proved that the printed T-joint-cut PENG is able to detect different pace frequency as well as gait posture, promising for the detection of slap gait and steppage gait caused by neurological diseases.

3. Conclusions

In conclusion, this work uses an all-3D printing method to form a stretchable kirigami structure PENG device, which provides a new way for fabricating piezoelectric device with functional structures that can be mounted into wearable textiles. Different from the widely used simple kirigami structure for stretching, this work designed a structure that can be pressed under large strain up to 300% without degradation in output voltage. The open current voltage of the PENG is 6 V, and the short circuit current is 2 $\mu A/cm^2$. The maximum power density is measured to be 1.4 $\mu W/cm^2$ when the load resistance is 10^7 Ω. The device can be mounted onto wearable textiles such as a sock to form an energy harvester that harvests the foot stamping energy and to act as a self-powered gait sensor. The T-joint-cut kirigami structure in this work innovatively enables the kirigami structured PENG to be stretched without severe out-of-plane deformation, which is crucial in the pressing mode PENGs. Furthermore, incorporating 3D printable electrodes also provides a facile way to fabricate an all-3D printed PENG, which simplifies the fabrication process. This all-3D printed kirigami based PENG can be applied as an energy harvester in wearable flexible and stretchable energy harvesting systems for self-powered electronic systems.

4. Material and methods

4.1. Materials and ink formation

$BaTiO_3$ NPs (Nanostructured & Amorphous Materials, Inc.) with diameter of around 200 nm and P(VDF-TrFE) (70-30 wt %) powders (Piezotech Arkema Group) are used as piezoelectric materials in this study. To form an ink for 3D printing, the P(VDF-TrFE) powder is dissolved into N, N-dimethylformamide (DMF, Sigma-Aldrich) by magnetic stirring at 300 rpm at 70 °C for 3 h with a concentration of 150 mg/ml. $BaTiO_3$ NPs were added to the P(VDF-TrFE) in DMF solution accordingly. The mixture was stirred for good dispersion and sonicated in a bath sonicator (S60H, Elmasonic) for 30 min for deagglomeration of the NPs. For the electrode ink formation, P(VDF-TrFE) is dissolved in methyl ethyl ketone (MEK, Emplura) at the same concentration. Silver flakes with weight ratio 2:1 to the P(VDF-TrFE) were added to the solution, followed by stirring and a 30-min sonication.

4.2. 3D printing

The 3D models were built with the software Inventor 2018 (Autodesk, Inc.). 3D printing was performed using an extrusion 3D printer System 30 M (Hyrel 3D, USA). This printer consists a printing head (SDS-5 Extruder) that holds a 1 ml syringe and a moving platform with heater. A piece of indium tin oxide (ITO) glass (Kaivo, ITO-P008) is put on the top of the platform as printing substrate. For printing, the piezoelectric ink is filled into the syringe with a needle that has a 0.26 mm inner diameter. The printing parameters are set in the printer as shown in Table 1. The build platform temperature was maintained at 70 °C for fast evaporating the solvent and solidify the composite. Five layers of ink was printed for a 40 μm thick sample. Then, the top electrode was printed onto the piezoelectric layer. The printing speed was lowered from 10 mm/s to 5 mm/s and the heating temperature is lowered to 50 °C. Two layers were printed for an electrode. After printing, the piezoelectric sample was annealed at 120 °C for 2 h. Then, it was poled with an amplifer/controller (Trek 610E H.V.) under 50 V/μm electric field and at 100 °C. The bottom electrode was then printed on the sample with the same printer and extruder. The printability was evaluated by comparing the feature size in the digital model and the printed device in Fig. S13.

4.3. Characterizations

The crystallographic phase of the materials was characterized by a powder X-ray diffractometer (XRD, Shimadzu XRD 7000) and a Fourier-transform infrared spectroscopy (FTIR, PerkinElmer Frontier). The morphology of the materials and samples were characterized with a field-emission scanning electron microscope (FESEM, JEOL 7600F). The mechanical properties were tested by a mechanical tester (Instron 5567) with tensile extension mode. The longitudinal mode piezoelectric coefficient (d_{33}) of the samples were tested by a standard static piezoelectric constant measuring instrument (Sinocera YE2730), and the energy harvesting performances were evaluated by analysing the output signals measured by a customized system including a function generator (Sinocera YE 1311), a signal amplifier (Sinocera YE5878), a magnetic shaker (Sinocera JZK-20), an oscilloscope (Tektronix MDO 3024), and a low noise current preamplifier (Stanford Research System, Model SR570). A force gauge was fixed on the shaker to measure the force that exerted on the sample (Sinocera CY-YD-303). The impedance of the samples was measured with a precision impedance analyser (Agilent 4294A). For the demonstration of gait analysis, the device was mounted on a cotton ribbed sock with a clay adhesive (Faber-Castell Tack-It). This

Table 1
Experimental parameters of 3D printing.

Slicing parameters	Conditions	3D printing parameters	Conditions
Layer height (mm)	0.04	Nozzle diameter (mm)	0.26
Print speed (mm/s)	10	Pulses (nL/sec)	2.3
Extrusion width (mm)	0.5	Flow rate	1
Perimeter extrusion width (mm)	0.3	Heating bed temperature (°C)	70

study was approved by the Institutional Review Board (IRB) at Nanyang Technological University (IRB-2017-08-038). Informed signed consent was obtained from all the participants.

4.4. Simulation

Finite element analysis was performed to the 3D model using the software Ansys 14.0 (ANSYS, Inc.). First, the 3D printing models built with Autodesk Inventor were imported into Ansys. Element type SOLID20 was considered and the models were divided into hexahedrons. The Young's modulus and Poisson's ratio were obtained from the tensile testing experiment, respectively to be 13.16 MPa and 0.5. All the structures were constrained with all degrees of freedom on the left surface and constrained with zero displacement in z-direction. 200 Pa pressure was applied on the right surface to all the structures along + x direction.

Declaration of competing interest

The authors declare no competing financial interests.

CRediT authorship contribution statement

Xinran Zhou: Conceptualization, Methodology, Visualization, Data curation, Writing - original draft. **Kaushik Parida:** Methodology, Validation, Resources, Writing - review & editing. **Oded Halevi:** Resources, Methodology. **Yizhi Liu:** Formal analysis. **Jiaqing Xiong:** Resources, Writing - review & editing. **Shlomo Magdassi:** Methodology, Supervision, Writing - review & editing. **Pooi See Lee:** Methodology, Supervision, Writing - review & editing.

Acknowledgement

This research is supported by the grant from the National Research Foundation, Prime Minister's Office, Singapore under its Campus of Research Excellence and Technological Enterprise (CREATE) programme.

Appendix A. Supplementary data

Supplementary data to this article can be found online at https://doi.org/10.1016/j.nanoen.2020.104676.

References

[1] G. Berndes, M. Hoogwijk, R. Van Den Broek, The contribution of biomass in the future global energy supply: a review of 17 studies, Biomass Bioenergy 25 (2003) 1–28, https://doi.org/10.1016/S0961-9534(02)00185-X.
[2] N. Armaroli, V. Balzani, The future of energy supply: challenges and opportunities, Angew. Chem. Int. Ed. 46 (2007) 52–66, https://doi.org/10.1002/anie.200602373.
[3] Y. Cui, C.M. Lieber, Functional nanoscale electronic devices assembled using silicon nanowire building blocks, Science 291 (80) (2001) 851–853, https://doi.org/10.1126/science.291.5505.851.
[4] P.D. Mitcheson, E.M. Yeatman, G.K. Rao, A.S. Holmes, T.C. Green, Energy harvesting from human and machine motion for wireless electronic devices, in: Proc. IEEE., vol. 96, 2008, pp. 1457–1486, https://doi.org/10.1109/JPROC.2008.927494.
[5] M. Salauddin, R.M. Toyabur, P. Maharjan, M.S. Rasel, J.W. Kim, H. Cho, J.Y. Park, Miniaturized springless hybrid nanogenerator for powering portable and wearable electronic devices from human-body-induced vibration, Nano Energy 51 (2018) 61–72, https://doi.org/10.1016/j.nanoen.2018.06.042.
[6] K.A. Cook-Chennault, N. Thambi, A.M. Sastry, Powering MEMS portable devices - a review of non-regenerative and regenerative power supply systems with special emphasis on piezoelectric energy harvesting systems, Smart Mater. Struct. 17 (2008), https://doi.org/10.1088/0964-1726/17/4/043001.
[7] E. Minazara, D. Vasic, F. Costa, Piezoelectric generator harvesting bike vibrations energy to supply portable devices, Renew. Energy Power Qual. J. 1 (2008) 508–513, https://doi.org/10.24084/repqj06.344.
[8] J.H. Lee, H.J. Yoon, T.Y. Kim, M.K. Gupta, J.H. Lee, W. Seung, H. Ryu, S.W. Kim, Micropatterned P(VDF-TrFE) film-based piezoelectric nanogenerators for highly sensitive self-powered pressure sensors, Adv. Funct. Mater. 25 (2015) 3203–3209, https://doi.org/10.1002/adfm.201500856.
[9] K.Y. Lee, M.K. Gupta, S.W. Kim, Transparent flexible stretchable piezoelectric and triboelectric nanogenerators for powering portable electronics, Nano Energy 14 (2015) 139–160, https://doi.org/10.1016/j.nanoen.2014.11.009.
[10] Y. Zang, F. Zhang, C.A. Di, D. Zhu, Advances of flexible pressure sensors toward artificial intelligence and health care applications, Mater. Horiz. 2 (2015) 140–156, https://doi.org/10.1039/c4mh00147h.
[11] F.R. Fan, W. Tang, Z.L. Wang, Flexible nanogenerators for energy harvesting and self-powered electronics, Adv. Mater. 28 (2016) 4283–4305, https://doi.org/10.1002/adma.201504299.
[12] V. Kumar, S. Park, K. Parida, V. Bhavanasi, P.S. Lee, Multi-responsive supercapacitors: smart solution to store electrical energy, Mater. Today Energy 4 (2017) 41–57, https://doi.org/10.1016/j.mtener.2017.03.004.
[13] H. Askari, A. Khajepour, M.B. Khamesee, Z. Saadatnia, Z.L. Wang, Piezoelectric and triboelectric nanogenerators: trends and impacts, Nano Today (2018), https://doi.org/10.1016/j.nantod.2018.08.001.
[14] J. Li, L. Kang, Y. Yu, Y. Long, J.J. Jeffery, W. Cai, X. Wang, Study of long-term biocompatibility and bio-safety of implantable nanogenerators, Nano Energy 51 (2018) 728–735, https://doi.org/10.1016/j.nanoen.2018.07.008.
[15] M.S. Rasel, P. Maharjan, M. Salauddin, M.T. Rahman, H.O. Cho, J.W. Kim, J. Y. Park, An impedance tunable and highly efficient triboelectric nanogenerator for large-scale, ultra-sensitive pressure sensing applications, Nano Energy 49 (2018) 603–613, https://doi.org/10.1016/j.nanoen.2018.04.060.
[16] X. Ren, H. Fan, C. Wang, J. Ma, H. Li, M. Zhang, S. Lei, W. Wang, Wind energy harvester based on coaxial rotatory freestanding triboelectric nanogenerators for self-powered water splitting, Nano Energy 50 (2018) 562–570, https://doi.org/10.1016/j.nanoen.2018.06.002.
[17] J.G. Sun, T.N. Yang, C.Y. Wang, L.J. Chen, A flexible transparent one-structure tribo-piezo-pyroelectric hybrid energy generator based on bio-inspired silver nanowires network for biomechanical energy harvesting and physiological monitoring, Nano Energy 48 (2018) 383–390, https://doi.org/10.1016/j.nanoen.2018.03.071.
[18] Y. Lee, S.H. Cha, Y.W. Kim, D. Choi, J.Y. Sun, Transparent and attachable ionic communicators based on self-cleanable triboelectric nanogenerators, Nat. Commun. 9 (2018), https://doi.org/10.1038/s41467-018-03954-x.
[19] Z.L. Wang, Triboelectric nanogenerators as new energy technology and self-powered sensors – principles, problems and perspectives, Faraday Discuss 176 (2014) 447–458, https://doi.org/10.1039/C4FD00159A.
[20] S.K. Ghosh, D. Mandal, Efficient natural piezoelectric nanogenerator: electricity generation from fish swim bladder, Nano Energy 28 (2016) 356–365, https://doi.org/10.1016/j.nanoen.2016.08.030.
[21] S.K. Ghosh, D. Mandal, Bio-assembled, piezoelectric prawn shell made self-powered wearable sensor for non-invasive physiological signal monitoring, Appl. Phys. Lett. 110 (2017) 123701, https://doi.org/10.1063/1.4979081.
[22] V. Bhavanasi, V. Kumar, K. Parida, J. Wang, P.S. Lee, Enhanced piezoelectric energy harvesting performance of flexible PVDF-TrFE bilayer films with graphene oxide, ACS Appl. Mater. Interfaces 8 (2016) 521–529, https://doi.org/10.1021/acsami.5b09502.
[23] X. Chen, K. Parida, J. Wang, J. Xiong, M.-F. Lin, J. Shao, P.S. Lee, A stretchable and transparent nanocomposite nanogenerator for self-powered physiological monitoring, ACS Appl. Mater. Interfaces (2017), https://doi.org/10.1021/acsami.7b13767 acsami.7b13767.
[24] S.K. Karan, D. Mandal, B.B. Khatua, Self-powered flexible Fe-doped RGO/PVDF nanocomposite: an excellent material for a piezoelectric energy harvester, Nanoscale 7 (2015) 10655–10666, https://doi.org/10.1039/C5NR02067K.
[25] J. Song, Z.L. Wang, Piezoelectric nanogenerators based on zinc oxide nanowire arrays, Science 312 (2006) 242–246.
[26] Y. Hu, Z.L. Wang, Recent progress in piezoelectric nanogenerators as a sustainable power source in self-powered systems and active sensors, Nano Energy 14 (2015) 3–14, https://doi.org/10.1016/j.nanoen.2014.11.038.
[27] S. Siddiqui, D. Il Kim, L.T. Duy, M.T. Nguyen, S. Muhammad, W.S. Yoon, N.E. Lee, High-performance flexible lead-free nanocomposite piezoelectric nanogenerator for biomechanical energy harvesting and storage, Nano Energy 15 (2015) 177–185, https://doi.org/10.1016/j.nanoen.2015.04.030.
[28] Q. Zheng, B. Shi, Z. Li, Z.L. Wang, Recent Progress on Piezoelectric and triboelectric energy harvesters in biomedical systems, Adv. Sci. 4 (2017) 1–23, https://doi.org/10.1002/advs.201700029.
[29] W.P. Mason, Piezoelectricity, its history and applications, J. Acoust. Soc. Am. 70 (1981) 1561–1566, https://doi.org/10.1121/1.387221.
[30] Y. Liu, W. Wu, W.A. Goddard, Tellurium: Fast Electrical and Atomic Transport along the Weak Interaction Direction, 2018, pp. 2–5, https://doi.org/10.1021/jacs.7b09964.
[31] S.K. Kim, R. Bhatia, T. Kim, D. Seol, J.H. Kim, H. Kim, W. Seung, Y. Kim, Y.H. Lee, S. Kim, Directional dependent piezoelectric effect in CVD grown monolayer MoS2 for flexible piezoelectric nanogenerators, Nano Energy 22 (2016) 483–489, https://doi.org/10.1016/j.nanoen.2016.02.046.
[32] Y. Zhou, W. Liu, X. Huang, A. Zhang, Y. Zhang, Z.L. Wang, Theoretical study on two-dimensional MoS2 piezoelectric nanogenerators, Nano Res. 9 (2016) 800–807, https://doi.org/10.1007/s12274-015-0959-8.
[33] T.R. Dargaville, M.C. Celina, J.M. Elliot, P.M. Chaplya, G.D. Jones, D.M. Mowery, R.A. Assink, R.L. Clough, J.W. Martin, Characterization, performance and optimization of PVDF as a piezoelectric film for advanced space mirror concepts, Sandia Natl. Lab. (2005). SAND2005-6846.
[34] F. Carpi, Electromechanically active polymers, Polym. Int. 59 (2010) 277–278, https://doi.org/10.1002/pi.2790.

[35] S. Garain, T. Kumar Sinha, P. Adhikary, K. Henkel, S. Sen, S. Ram, C. Sinha, D. Schmeißer, D. Mandal, Self-poled transparent and flexible UV light-emitting cerium complex-PVDF composite: a high-performance nanogenerator, ACS Appl. Mater. Interfaces 7 (2015) 1298–1307, https://doi.org/10.1021/am507522r.
[36] D.Y. Kusuma, C.A. Nguyen, P.S. Lee, Enhanced ferroelectric switching characteristics of P(VDF-TrFE) for organic memory devices, J. Phys. Chem. B 114 (2010) 13289–13293, https://doi.org/10.1021/jp105249f.
[37] A. Chortos, Z. Bao, Skin-inspired electronic devices, Mater, Today 17 (2014) 321–331, https://doi.org/10.1016/j.mattod.2014.05.006.
[38] Y. Qi, J. Kim, T.D. Nguyen, B. Lisko, P.K. Purohit, M.C. McAlpine, Enhanced piezoelectricity and stretchability in energy harvesting devices fabricated from buckled PZT ribbons, Nano Lett. 11 (2011) 1331–1336, https://doi.org/10.1021/nl104412b.
[39] Y. Duan, Y. Huang, Z. Yin, N. Bu, W. Dong, Non-wrinkled, highly stretchable piezoelectric devices by electrohydrodynamic direct-writing, Nanoscale 6 (2014) 3289, https://doi.org/10.1039/c3nr06007a.
[40] Y. Duan, Y. Ding, J. Bian, Z. Xu, Z. Yin, Y. Huang, Ultra-stretchable piezoelectric nanogenerators via large-scale aligned fractal inspired micro/nanofibers, Polymers 9 (2017) 1–11, https://doi.org/10.3390/polym9120714.
[41] D. Yun, K.-S. Yun, Woven piezoelectric structure for stretchable energy harvester, Electron. Lett. 49 (2013) 65–66, https://doi.org/10.1049/el.2012.3712.
[42] J.H. Lee, K.Y. Lee, M.K. Gupta, T.Y. Kim, D.Y. Lee, J. Oh, C. Ryu, W.J. Yoo, C. Y. Kang, S.J. Yoon, J.B. Yoo, S.W. Kim, Highly stretchable piezoelectric-pyroelectric hybrid nanogenerator, Adv. Mater. 26 (2014) 765–769, https://doi.org/10.1002/adma.201303570.
[43] C.K. Jeong, J. Lee, S. Han, J. Ryu, G.T. Hwang, D.Y. Park, J.H. Park, S.S. Lee, M. Byun, S.H. Ko, K.J. Lee, A hyper-stretchable elastic-composite energy harvester, Adv. Mater. 27 (2015) 2866–2875, https://doi.org/10.1002/adma.201500367.
[44] X. Chou, J. Zhu, S. Qian, X. Niu, J. Qian, X. Hou, J. Mu, W. Geng, J. Cho, J. He, C. Xue, All-in-one filler-elastomer-based high-performance stretchable piezoelectric nanogenerator for kinetic energy harvesting and self-powered motion monitoring, Nano Energy 53 (2018) 550–558, https://doi.org/10.1016/j.nanoen.2018.09.006.
[45] X. Niu, W. Jia, S. Qian, J. Zhu, J. Zhang, X. Hou, J. Mu, W. Geng, J. Cho, J. He, X. Chou, High-performance PZT-based stretchable piezoelectric nanogenerator, ACS Sustain. Chem. Eng. 7 (2019) 979–985, https://doi.org/10.1021/acssuschemeng.8b04627.
[46] N. Hu, D. Chen, D. Wang, S. Huang, I. Trase, H.M. Grover, X. Yu, J.X.J. Zhang, Z. Chen, Stretchable kirigami polyvinylidene difluoride thin films for energy harvesting: design, analysis, and performance, Phys. Rev. Appl. 9 (2018) 21002, https://doi.org/10.1103/PhysRevApplied.9.021002.
[47] Z. Lv, Y. Luo, Y. Tang, J. Wei, Z. Zhu, X. Zhou, W. Li, Y. Zeng, W. Zhang, Y. Zhang, D. Qi, S. Pan, X.J. Loh, X. Chen, Editable supercapacitors with customizable stretchability based on mechanically strengthened ultralong MnO_2 nanowire Composite, Adv. Mater. 1704531 (2017) 1704531, https://doi.org/10.1002/adma.201704531.
[48] A. Lamoureux, K. Lee, M. Shlian, S.R. Forrest, M. Shtein, Dynamic kirigami structures for integrated solar tracking, Nat. Commun. 6 (2015) 1–6, https://doi.org/10.1038/ncomms9092.
[49] A. Baldwin, E. Meng, A kirigami-based Parylene C stretch sensor, Proc. - IEEE Int. Conf. Micro Electro Mech. Syst. (MEMS) (2017) 227–230, https://doi.org/10.1109/MEMSYS.2017.7863382.
[50] R. Sun, B. Zhang, L. Yang, W. Zhang, I. Farrow, F. Scarpa, J. Rossiter, Kirigami stretchable strain sensors with enhanced piezoelectricity induced by topological electrodes, Appl. Phys. Lett. 112 (2018) 1–6, https://doi.org/10.1063/1.5025025.
[51] F. Rengier, A. Mehndiratta, H. Von Tengg-Kobligk, C.M. Zechmann, R. Unterhinninghofen, H.U. Kauczor, F.L. Giesel, 3D printing based on imaging data: review of medical applications, Int. J. Comput. Assist. Radiol. Surg. 5 (2010) 335–341, https://doi.org/10.1007/s11548-010-0476-x.
[52] S. Bose, S. Vahabzadeh, A. Bandyopadhyay, Bone tissue engineering using 3D printing, Mater. Today 16 (2013) 496–504, https://doi.org/10.1016/j.mattod.2013.11.017.
[53] K. Kim, W. Zhu, X. Qu, C. Aaronson, W.R. McCall, S. Chen, D.J. Sirbuly, 3D optical printing of piezoelectric nanoparticle-polymer composite materials, ACS Nano 8 (2014) 9799–9806, https://doi.org/10.1021/nn503268f.
[54] A. Marino, J. Barsotti, G. De Vito, C. Filippeschi, B. Mazzolai, V. Piazza, M. Labardi, V. Mattoli, G. Ciofani, Two-photon lithography of 3D nanocomposite piezoelectric scaffolds for cell stimulation, ACS Appl. Mater. Interfaces 7 (2015) 25574–25579, https://doi.org/10.1021/acsami.5b08764.
[55] D.A. Porter, T.V.T. Hoang, T.A. Berfield, Effects of in-situ poling and process parameters on fused filament fabrication printed PVDF sheet mechanical and electrical properties, Addit. Manuf. 13 (2017) 81–92, https://doi.org/10.1016/j.addma.2016.11.005.
[56] X. Chen, H.O.T. Ware, E. Baker, W. Chu, J. Hu, C. Sun, The development of an all-polymer-based piezoelectric photocurable resin for additive manufacturing, Procedia CIRP 65 (2017) 157–162, https://doi.org/10.1016/j.procir.2017.04.025.
[57] C.X.F. Lam, X.M. Mo, S.H. Teoh, D.W. Hutmacher, Scaffold development using 3D printing with a starch-based polymer, Mater. Sci. Eng. C 20 (2002) 49–56, https://doi.org/10.1016/S0928-4931(02)00012-7.
[58] B.M.D. Waugh, Design Solutions for DC Bias in Multilayer Ceramic Capacitors, 2010, pp. 34–36.
[59] A.K. Batra, M.E. Edwards, A. Alomari, A. Elkhaldy, Dielectric behavior of P(VDF-TrFE)/PZT nanocomposites films doped with multi-walled carbon nanotubes (MWCNT), Am. J. Mater. Sci. 5 (2015) 55–61, https://doi.org/10.5923/s.materials.201502.09.
[60] V. Kunin, S. Yang, Y. Cho, P. Deymier, D.J. Srolovitz, Static and dynamic elastic properties of fractal-cut materials, Extrem. Mech. Lett. 6 (2016) 103–114, https://doi.org/10.1016/j.eml.2015.12.003.
[61] Y. Cha, K. Song, J. Shin, D. Kim, Gait analysis system based on slippers with flexible piezoelectric sensors, in: IEEE Int. Conf. Robot. Biomimetics, ROBIO 2018, 2018, pp. 2479–2484, https://doi.org/10.1109/ROBIO.2018.8664872, 2019.
[62] N.B. Alexander, A. Goldberg, Gait disorders : search for multiple causes, Cleve, Clin. J. Med. 72 (2005) 586–600.
[63] N. Itoh, D. Imoto, S. Kubo, K. Takahashi, N. Hishikawa, Y. Mikami, T. Kubo, Gait training using a stationary, one-leg gait exercise assist robot for chronic stroke hemiplegia: a case report, J. Phys. Ther. Sci. 30 (2018) 1046–1051, https://doi.org/10.1589/jpts.30.1046.
[64] N. Koceska, S. Koceski, Review: robot devices for gait rehabilitation, Int. J. Comput. Appl. 62 (2013) 1–8, https://doi.org/10.5120/10137-4279.
[65] Z. Zhang, Z. Zhu, B. Bazor, S. Lee, Z. Ding, T. Pan, FeetBeat: a flexible iontronic sensing wearable detects pedal pulses and muscular activities, IEEE Trans. Biomed. Eng. 9294 (2019), https://doi.org/10.1109/tbme.2019.2900224, 1–1.
[66] M. de F. Domingues, C. Tavares, T. Leite, N. Alberto, C. Leitão, C. Marques, A. Radwan, E. Rocon, P. Antunes, P. André, Fiber Bragg gratings as e-health enablers: an overview for gait analysis applications, Heavy Met. Remov. with Phytoremediation., i, 13, https://doi.org/10.5772/57353, 2016.
[67] J. Yu, X. Hou, M. Cui, S. Zhang, J. He, W. Geng, J. Mu, X. Chou, Highly skin-conformal wearable tactile sensor based on piezoelectric-enhanced triboelectric nanogenerator, Nano Energy 64 (2019) 103923, https://doi.org/10.1016/j.nanoen.2019.103923.